



# A low-complexity transceiver scheme for joint DFT pre-coded DWT SC-FDMA NOMA system under dissimilar power allocation strategies

M SUBHA<sup>1</sup> and D JUDSON<sup>2,\*</sup> 

<sup>1</sup>Department of Electronics and Communication Engineering, University College of Engineering Nagercoil, Nagercoil, Tamil Nadu 629004, India

<sup>2</sup>Department of Electronics and Communication Engineering, SRM Valliammai Engineering College, SRM Nagar, Kattankulathur, Tamil Nadu 603203, India  
e-mail: judson\_d2001@yahoo.co.in

MS received 29 July 2023; revised 5 March 2024; accepted 22 April 2024

**Abstract.** The competence of Non-Orthogonal Multiple Access (NOMA) to provide improved spectrum efficiency, support massive network elements, and low latency services make it attractive to Multiple Access (MA) technology for next-generation wireless networks. Single-Carrier Frequency Division Multiple Access (SC-FDMA) is an optimal technique in 4G wireless communication to enhance spectrum efficiency and user capacity. The amalgamation of SC-FDMA with NOMA can become a better choice for wireless communication for 5G and Beyond 5G (B5G). Discrete Wavelet Transforms (DWT) have been a better choice for improving the system's performance due to its outstanding orthogonality and spectral confinement characteristics. This study proposes a transceiver architecture that uses joint Discrete Fourier Transform (DFT) and DWT to outperform existing NOMA systems in terms of Bit Error Rate (BER). The transceiver architecture is symbolized as a joint DFT precoded DWT (JDPD) SC-FDMA NOMA System. Furthermore, we propose a Joint Low Complexity Regularized Zero forcing (JLC RZF) for JDPD SC-FDMA NOMA system to enhance the BER with low complexity. In order to illustrate the superiority of the proposed system over multipath channels, the system performance over a range of Carrier Frequency Offset (CFO) values and power allocation scenarios are also examined.

**Keywords.** NOMA; SC-FDMA; Precoded DFT; DWT; Carrier frequency offset.

## 1. Introduction

To support extremely high data rates, various applications and services are integrated into 5G and Beyond 5G B5G [1]. However, Multiple Access (MA) systems, common in earlier cellular system generations, will need to be more competent to meet the exceptional network throughput and user density demands of the forthcoming wireless systems. Since migrating from generation to generation, MA systems significantly distinguish between various wireless methods. Frequency-Division Multiple Access (FDMA) was the primary Orthogonal multiple access (OMA) method used in the 1G cellular network. The key emphasis of the 2G communication was Time-Division Multiple Access (TDMA). Code-Division Multiple Access (CDMA) remained a major MA in 3G, whereas 4G used Orthogonal FDMA (OFDMA).

“Orthogonality” is the problem that collectively affects all MA systems. In an ideal world, different users would continue to use distinct sub channels, resource elements,

spreading sequences, and time slots [2]. As a result, orthogonality is intended to safeguard itself while traveling through the wireless network without hindering other users. This privilege of orthogonality restricts the size of network elements subscribers can employ, this leads to reduction of overall spectral efficiency. The most intriguing aspect of Non-Orthogonal Multiple Access (NOMA) systems is allowing several user elements to share the same subcarrier while maintaining them apart through increased receiver complexity [3]. NOMA enables overlapping signals from different nodes by utilizing the three domains, namely power, code, and interleaving pattern [4]. By using Power Domain Multiplexing at the transmitter, NOMA retrieves transmitted data at the Base Station (BS) via Successive Interference Cancellation (SIC). The prospects and difficulties of NOMA used in downlink systems for cellular communication were discussed in [5, 6]. According to research on the user combination effect for NOMA in [7], performance improves once a strong user is amalgamated with a weak user for downlink transmissions.

There has been significant interest in Single Carrier (SC) systems with Frequency Domain Equalization (FDE)

\*For correspondence  
Published online: 27 June 2024

offering greater data rate. Although SC-FDE and OFDM have similar operational complexity and lower Peak to Average Power Ratio (PAPR) [8], the greater PAPR in OFDM has augmented the necessity of developing a different transmission scheme for LTE uplink. This resulted in SC-FDMA communication system [9–11]. At mobile units, NOMA and OFDM offer significant spectral efficiency and fairness index performance improvements [12]. In order to reduce PAPR, Discrete Fourier Transform (DFT)-based precoding was employed in OFDM systems [13], which led SC-FDMA to become a key MA technique in 3GPP LTE [14]. In [15, 16], the theoretical feasibility of a generalized precoding matrix based on Discrete Hartley Transform (DHT), Discrete Cosine Transform (DCT), and DFT was investigated. For lowering PAPR in NOMA-OFDM systems, Discrete Sine Transform (DST) and DCT-based precoding approaches have been investigated [17].

OFDMA and other OMA algorithms cannot exceed the system capacity limit of the uplink because of the resource distribution exclusivity. When the system considers user fairness, this problem becomes more obvious. In order to help users, separate their signals at the receiver using current NOMA techniques, redundancy is introduced by coding and spreading. However, redundancy reduces the system's spectral efficiency. Therefore, more effective NOMA schemes must be created in order to reach higher capacity. Based on this, Bachl *et al* [12] presented a NOMA uplink system that eliminates the restriction on resource allocation and permits several users to share a single subcarrier without coding or spreading redundancy. The receiver employs joint processing to recognize user signals. A brand-new subcarrier and power distribution method that maximizes users' sum rate is also suggested for NOMA scheme.

There are some drawbacks peculiar to multicarrier NOMA. For standardization to be effective, these weaknesses need to be addressed carefully. One of the main issues, among others, is the PAPR issue. Discrete-Cosine Transform Matrix (DCTM) precoding is achieved by adding a new precoding block [18]. The DCTM precoder uses the multipath fading channel to disperse information, which lowers the Bit Error Rate (BER). In order to reduce the higher PAPR, the DST matrix precoding based uplink NOMA technique has been suggested in Yang *et al* [19]. In Li *et al* [20], the author compares six precoding matrices from the literature. The findings demonstrated that, except for square-root raised cosine function, all precoding matrices remain ineffective in terms of BER performance. DCT precoded real domain OFDM can offer doubled subcarriers for low order modulation like Binary Phase Shift Keying (BPSK) when compared to discrete Fourier transform matrix spreading OFDM in the same bandwidth [21]. SC-FDMA is proposed for use with NOMA in [22], where the authors propose clustering of user cells and subband allocation to improve cell edge throughput and overall throughput. According to the authors in [23],

NOMA with imperfect SIC performed well on the BER test. Frequency reuse is used for an asynchronous uplink in a new interference cancellation strategy for NOMA, according to Al-kamali *et al* [24]. BER performance can be significantly enhanced using the SIC method.

Wavelet-based NOMA systems have continued to be the main focus for downlink communication [25]. A new transceiver design uses Discrete Wavelet Transform (DWT) to separate the transferred data into approximation and detail components for SC-FDMA systems. Due to its sensitivity to noise, the detail component is left unaltered, while the approximation component can be cut or combined. At both the transmitter and the receiver, wavelet filter banks show the capacity to lessen distortion while preserving all of the important signal characteristics. The companding, clipping, and hybrid methods are recommended for lowering PAPR although retaining BER performance.

Most experimental studies of NOMA-OFDM systems have yet to study the performance under Carrier Frequency Offset (CFO) deviations at the receiver [26]. Furthermore, a different precoding technique that combines wavelet transforms with DFT-based precoding was not considered for SC-FDMA NOMA systems [27]. The equalization techniques employed in the receiver are commonly categorized into Zero-Forcing (ZF), Minimum Mean Square Error (MMSE) and Regularized Zero Forcing (RZF). The MMSE more efficiently equalizes the received signal with the SNR and interference matrix. However, RZF performs equalization with lower complexity without the interference matrix and noise [28]. In Khan *et al* [29], the authors analysed a Joint Low Complexity RZF (JLC-RZF) using Banded Matrix Approximation (BMA). The use of BMA achieves performance close to full compensation with less complexity. The paper is structured as follows:

- We begin explaining the NOMA system with the framework of SC-FDMA system with DFT-based precoding combined with NOMA and then its analysis.
- The proposed transceiver for SC-FDMA NOMA system employing joint DFT precoding and DWT is investigated to display the extraordinary BER performance over the traditional systems. The recommended transceiver architecture is stated as joint DFT precoded DWT (JDPD) SC-FDMA NOMA.
- We propose a JLC-RZF for JDPD SC-FDMA NOMA system using low complexity BMA to show its excellent capability in improving the BER performances compared to the existing DFT SC-FDMA NOMA system using a MMSE receiver structure. We also validate BER performance with CFO variations under this paper's constraint.
- The complex nature of the multipath channel is of significant interest in NOMA systems and multipath channel plays a prominent role in allocating power among users in a cluster. Moreover, the power

allocation between the strong and weak users achieves the desired BER performance. Hence, this paper analyzes the BER performance of the proposed JDPD SC-FDMA NOMA using different power allocation strategies and portrays the proposed system's significance.

The remaining part of this paper is formulated as follows: The operation and analysis of the DFT SC-FDMA NOMA system are covered in section 2. In section 3, it is demonstrated how the SC-FDMA NOMA system is jointly equalized with several equalization techniques with CFO. Section 4 analyzes the proposed JDPD SC-FDMA NOMA system. The simulation results are discussed in section 5, demonstrating their significance in enhancing BER performance. Finally, the conclusions are provided in section 6.

## 2. DFT precoded SC-FDMA NOMA

The system model of a conventional SC-FDMA NOMA system with DFT precoding is depicted in figure 1. The system consists of  $K$  uplink users, who are homogeneously scattered in a cellular system. The modulated data blocks are separated into blocks of size  $N$ , and DFT is spread to each input data block. Here, the data is processed in the time and frequency domains using DFT/IDFT blocks. The orthogonality among the subcarriers is maintained by assigning the same set of subcarriers to  $l$  users in a cluster.

The total number of clusters obtained is  $P = K/l$ . The subcarriers in each cluster are allocated using localized mapping and passed through the IDFT module to convert the frequency domain signal into time domain [29]. The cyclic prefix (CP) is added after the IDFT module, and the

data from  $k^{\text{th}}$  user of  $p^{\text{th}}$  cluster is transmitted over the wireless channel denoted as

$$x_l(m) = \frac{1}{N} \sum_{n=0}^{N-1} \sum_{k=(p-1)l+1}^{pl} \sqrt{\alpha_k} x_k^p(n) e^{(j2\pi/N)mn}. \quad (1)$$

In Equation (1)  $l$  represents the user size in  $p^{\text{th}}$  cluster.  $\alpha_k$  is the fractional power assigned to  $k^{\text{th}}$  user and  $m = 0, 1, \dots, N - 1$ . The total signal radiated from all the clusters to the BS is denoted as

$$x(m) = \sum_{p=1}^P \frac{1}{N} \sum_{n=0}^{N-1} \sum_{k=(p-1)l+1}^{pl} \sqrt{\alpha_k} x_k^p(n) e^{(j2\pi/N)mn}. \quad (2)$$

The transmitted signal that propagates over multipath channel experiences a linear convolution between the channel impulse responses taking  $L$  independent paths. This causes Intersymbol Interference (ISI) between each serial transmitted data in the time domain. The CFO induced signal at the receiver is represented as

$$y(m) = \sum_{p=1}^P \sum_{k=(p-1)l+1}^{pl} (x_k^p(m) \otimes h_k^p(m)) e^{(j2\pi \epsilon_k m/M)} + N(m). \quad (3)$$

In equation (3)  $h_k^p(m)$  is the  $L$  tap channel impulse response for  $k^{\text{th}}$  user of  $p^{\text{th}}$  cluster denoted as

$$h_k^p(m) = \sum_{i=0}^{L-1} h_i \delta(m - \tau_i). \quad (4)$$

Here  $h_i$  and  $\tau_i$  resemble the gain of  $i^{\text{th}}$  resolvable path and delay spread of multipath channel.  $\epsilon_k$  defines the normalized CFO of  $k^{\text{th}}$  user.  $N(m)$  is the Additive White Gaussian Noise (AWGN). CFO causes performance degradation

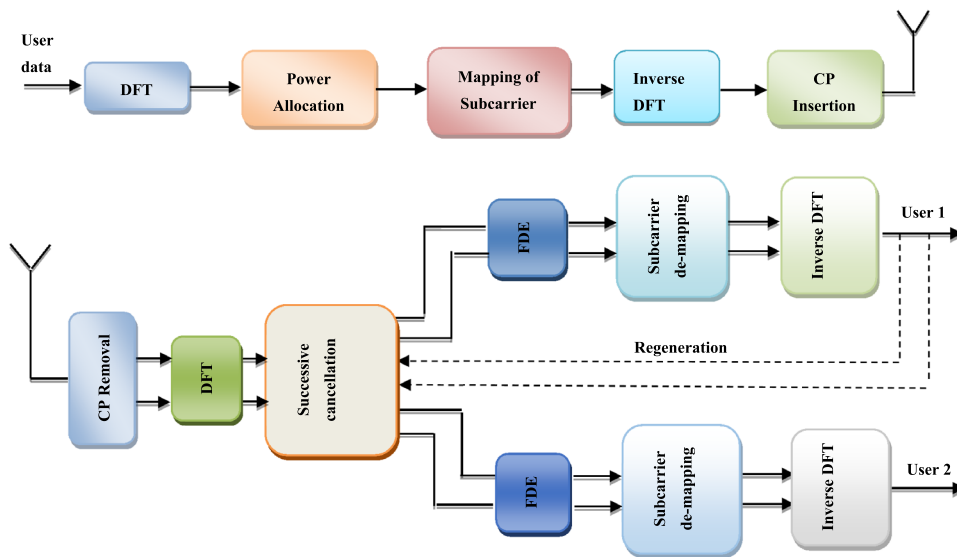


Figure 1. System model of SC-FDMA NOMA System.

during detection of desired user data due to Intercarrier Interference (ICI) and Multiple Access Interference (MAI). Hence CFO compensation and equalization plays an important part in mitigating the interference in SC-FDMA NOMA system. After removal of CP and applying DFT [30], the frequency domain equivalent for user  $k$  in  $p^{\text{th}}$  cluster is formulated in terms of interference and desired signal as

$$\begin{aligned}
Y_k^p(u) &= \sum_{u \in \phi_p} \sqrt{\alpha_i} X_k^p(u) H_k^p(u) \eta(u, u, \epsilon_k) \\
&+ \sum_{\substack{u \in \phi_p \\ v \neq u}} \sqrt{\alpha_k} X_k^p(u) H_k^p(u) \eta(u, v, \epsilon_k) \\
&+ \sum_{u \in \phi_p} \sum_{\substack{j = (p-1)l+1 \\ j \neq k}}^{pl} \sqrt{\alpha_j} X_j^p(u) H_j^p(u) \eta(u, u, \epsilon_j) + N(u)
\end{aligned} \tag{5}$$

In the above equation, the desired user data with interference is defined in the first term, the second term is due to ICI triggered by CFO, the next term is caused by the ICI due to CFO triggered by other users occupying the same set of subcarriers in the  $p^{\text{th}}$  cluster. Finally, the last term is the AWGN.  $\phi_p$  characterizes the set of subcarriers assigned to  $p^{\text{th}}$  cluster.  $\eta(u, v, \epsilon)$  denotes the interference produced by CFO resulting in ICI from different subcarriers upon the desired subcarrier specified as [10, 11, 31]

$$\eta(u, v, \epsilon) = \xi \frac{\sin(\pi(v - u + \epsilon))}{N \sin\left(\frac{\pi(v - u + \epsilon)}{N}\right)} \tag{6}$$

where  $\xi = \exp(j\pi(v - u + \epsilon)) \frac{(N-1)}{N} \cdot (v - u)$  denotes the relative subcarrier distance.

### 3. Joint DFT precoding and DWT in SC-FDMA NOMA

DWT exhibits perfect reconstruction of transmitted information by reconstructing the decomposed waveform without worsening the waveform's spectral characteristics. DWT decomposes the input signal into detail and approximation components. DWT is performed from the discrete time signals through low pass filter (LPF) and high pass filter (HPF). The HPF generates the detail component, and the LPF generates the coarse approximation component and continues until the required decomposition stage is achieved. The DWT is obtained by multiplexing the detail and approximation coefficients from the last stage to the first stage of decomposition [26]. Finally, reconstructions of

the original signal are obtained by synthesizing the original signal by LPF and HPF and using the same amount of synthesis stages as done during decomposition.

In this paper, the Haar wavelet is considered for analysis of wavelet transform. The architecture of the proposed JDPD SC-FDMA NOMA system is shown in figure 2. The DFT output is subjected to localized mapping and allocated with its corresponding user power. After subcarrier mapping, IDFT is performed to obtain the signal as given in Equation (1). In JDPD SC-FDMA NOMA system, DWT is realized using two-channel filter banks using an ordered pyramidal algorithm [31]. The IDFT modulated samples are applied to the DWT block. The block generates factors corresponding to scaling and wavelet transform coefficients denoted as

$$\begin{aligned}
\lambda_{\alpha, \beta} &= \langle X^k[u], \varphi_{\alpha, \beta}[u] \rangle \\
&= \frac{1}{\sqrt{M}} \sum_n X^k[u] \varphi_{\alpha, \beta}[u] \\
\lambda_{\alpha, \beta} &= \langle X^k[u], \phi_{\alpha, \beta}[u] \rangle \\
&= \frac{1}{\sqrt{M}} \sum_n X^k[u] \phi_{\alpha, \beta}[u] \\
&= \frac{1}{\sqrt{M}} \sum_n X^k[u] 2^{\alpha/2} \phi_{\alpha, \beta}[2^\alpha u - \beta]
\end{aligned} \tag{7}$$

$$\begin{aligned}
\gamma_{\alpha, \beta} &= \langle X^k[u], \psi_{\alpha, \beta}[u] \rangle \\
&= \frac{1}{\sqrt{M}} \sum_n X^k[u] \psi_{\alpha, \beta}[u], \\
\gamma_{\alpha, \beta} &= \langle X^k[u], \psi_{\alpha, \beta}[u] \rangle \\
&= \frac{1}{\sqrt{M}} \sum_n X^k[u] \psi_{\alpha, \beta}[u] \\
&= \frac{1}{\sqrt{M}} \sum_n X^k[u] 2^{\alpha/2} \psi_{\alpha, \beta}[2^\alpha u - \beta]
\end{aligned} \tag{8}$$

where  $\frac{1}{\sqrt{M}}$  is the normalization factor based on the resolution of  $\alpha$  and is determined using  $M = 2^\alpha$ .  $\alpha$  and  $\beta$  are the scaling and shift parameters considered as an integer. The subsequent signal corresponding to scaling and wavelet filter coefficients of  $k^{\text{th}}$  user of  $p^{\text{th}}$  cluster is multiplexed and added with CP and send over the wireless channel. The CFO induced signal at the BS is represented as

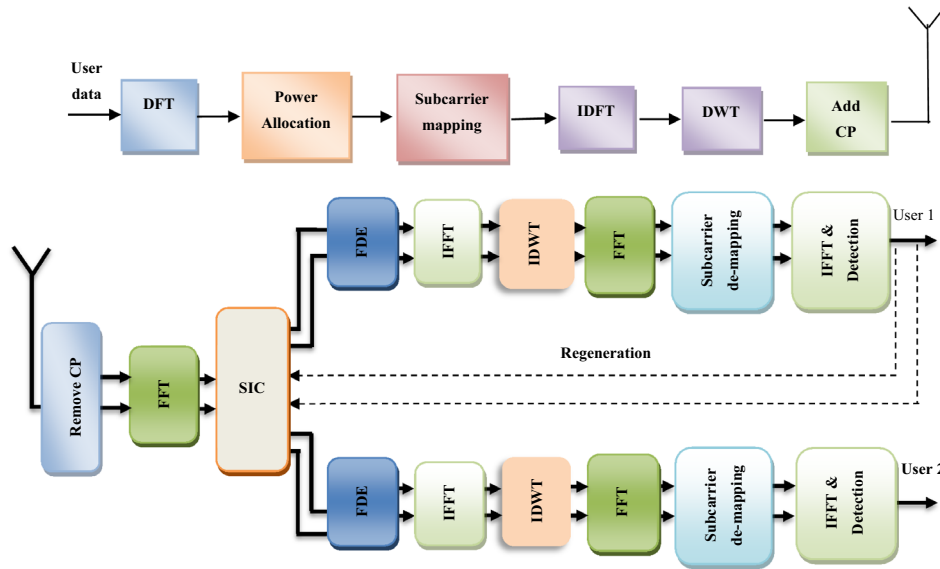


Figure 2. System Model of JDPD SC-FDMA NOMA.

$$y_{DWT}(m) = \sum_{p=1}^P \sum_{k=(p-1)l+1}^{pl} (X_{DWT,k}^p(m) * h_k^p(m)) e^{j2\pi\epsilon_k m/M} + N(m), \quad (9)$$

where,  $X_{DWT,k}^p$  represents the multiplexed scaling and wavelet filter coefficients radiated from  $k^{\text{th}}$  user of  $p^{\text{th}}$  cluster.

The CP removed signal is subjected to M-point DFT to obtain a frequency domain signal for performing FDE. Then, the FDE and CFO elimination is achieved jointly to reconstruct the user data at the receiver side of the JDPD SC-FDMA NOMA system [32]. Many literatures investigated various equalization techniques for improving system performance, including joint equalization and CFO compensation [33]. The weights associated with joint equalization and CFO elimination vector for  $k^{\text{th}}$  user belonging to cluster  $p$  is represented as

$$W_{k,ZF}^p = \left( (\psi_k^p)^H \psi_k^p \right)^{-1} (\psi_k^p)^{-1}, \quad (10)$$

In Equation (7)  $\psi_k^p = \pi_k^p \eta(u, v, \epsilon_k)$ .  $\pi_k^p$  is the channel matrix of  $k^{\text{th}}$  user belonging to  $p^{\text{th}}$  cluster with size  $N \times N$ .  $\eta(u, v, \epsilon_k)$  is the CFO matrix. The ZF equalizer performance is deteriorated due to noise amplification and MAI. MMSE equalizer reduces the noise amplification due to the inclusion of noise approximation parameters in the equalizer weights. The MMSE weights is given by

$$W_{k,MMSE}^p = \left( (\psi_k^p)^H \psi_k^p + \frac{1}{SNR} I_{M \times M} \right)^{-1} (\psi_k^p)^H, \quad (11)$$

where  $I_{M \times M}$  is an identity matrix. In MMSE equalizer the interference due to noise is eliminated by means of estimated noise component. Based on ZF and MMSE equalization, the frequency domain signal is equalized to acquire the  $k^{\text{th}}$  user data of  $p^{\text{th}}$  cluster as

$$\hat{Y}_{DWT,k}^{(p)} = Y_{DWT,k}^{(p)} W_{k,MMSE}^p. \quad (12)$$

Using the MMSE equalization weights in (12), the  $k^{\text{th}}$  user equalized signal for subcarrier  $u$  belonging to  $p^{\text{th}}$  cluster is denoted as

$$\begin{aligned} \hat{Y}_{DWT,i}^{(p)}(u) &= \sqrt{\alpha_i} \sum_{u \in \phi_p} X_{DWT,i}^p(u) \Psi_i^p(u) (\Theta(u))^{-1} (\psi_i^p(u))^H \\ &+ \sqrt{\alpha_i} \sum_{\substack{v \in \phi_p \\ v \neq u}} X_{DWT,i}^p(v) \Psi_i^p(v) (\Theta(v))^{-1} (\psi_i^p(u))^H \\ &+ \sum_{u \in \phi_p} \sum_{\substack{j=(p-1)l+1 \\ j \neq i}}^{pl} \sqrt{\alpha_j} X_{DWT,j}^p(u) \Psi_i^p(u) (\Theta(u))^{-1} \\ &(\psi_i^p(u))^H + \Psi_i^p(u) (\Theta(u))^{-1} N(u) (\psi_i^p(u))^H, \end{aligned} \quad (13)$$

where



$$\begin{aligned}\Theta(u) &= (\Psi_i^p(u))^H \Psi_i^p(u) + (1/SNR)I_{M \times M} \\ \Theta(v) &= (\Psi_i^p(v))^H \Psi_i^p(v) + (1/SNR)I_{M \times M}.\end{aligned}$$

Simplifying the above equation, we obtain the equalized signal in terms of desired data, ICI, intra cluster interference and noise as given below

$$\begin{aligned}\hat{Y}_{DWT,i}^{(p)}(u) &= \underbrace{\sqrt{\alpha_i} \sum_{u \in \phi_p} X_{DWT,i}^p(u) \delta_i(u)}_{\text{desired signal}} \\ &+ \underbrace{\sqrt{\alpha_i} \sum_{\substack{v \in \phi_p \\ v \neq u}} X_{DWT,i}^p(v) \delta_i(v)}_{\text{intercarrier interference}} \\ &+ \underbrace{\sum_{u \in \phi_p} \sum_{\substack{j = (p-1)l + 1 \\ j \neq i}} \sqrt{\alpha_j} X_{DWT,j}^p(u) \delta_i(u)}_{\text{intracluster interference}} \\ &+ \underbrace{\bar{N}(u)}_{\text{additive noise}},\end{aligned}\tag{14}$$

where  $\bar{N}(u) = \psi_i^p(u) \left( (\psi_i^p(u))^H \psi_i^p(u) + (1/SNR)I_{M \times M} \right)^{-1} N(u)$ , and  $\delta_i(\cdot)$  denotes the residual interference. It is noted from equation (14) that the perfect estimation of noise in MMSE equalization determines the accuracy of detection in the proposed system. The equalized signal is applied to the IFFT block to acquire the time domain signal and demultiplexed to separate the scaling and wavelet filter coefficients. The signal is then applied to the IDWT block to obtain the inverse transformed signal as given by

$$X_{IDWT,p}^k = \frac{1}{\sqrt{M}} \sum_{\beta=-\infty}^{\infty} \lambda_{\alpha,\beta} \phi_{\alpha,\beta}[n] + \sum_{\alpha=-\infty}^{\infty} \sum_{\beta=-\infty}^{\infty} \gamma_{\alpha,\beta} \psi_{\alpha,\beta}[n].\tag{15}$$

The IDWT output is applied to IFFT module to acquire the frequency domain signal. Then the output signal from IDWT module is demapped using the subcarrier demapping matrix. The demapped data undergoes inverse precoding using the matrix  $F_M^{-1} F_M^{-1}$  to obtain the detected data for the  $k^{\text{th}}$  user of  $p^{\text{th}}$  cluster as

$$\hat{x}_k^p = \text{sgn} \left( F_M^{-1} \left( X_k^{(p)}(u) \right) \right).\tag{16}$$

The data of strong user is estimated thus, to detect the weak user data, the strong user in the  $p$ -th cluster is regenerated based on the precoding matrix, estimated

channel coefficients, interference matrix, and user power. After regeneration, SIC is employed to recover the weak user data. SIC is the finest detection technique in CDMA systems in uplink transmissions when the transmitted data is affected by near-far effect [34]. In JDPD SC-FDMA NOMA, the regenerated strong user data is cancelled from the received complex signal using SIC to detect the weak user. The SIC is done in the frequency domain as

$$Y_{i+1}^p(u) = Y^{(p)}(u) - \psi_i^p D_M \left\{ F_M^{-1} \left\{ F_N \left( \hat{x}_k^p \right) \right\} \right\},\tag{17}$$

where  $Y^{(p)}(u)$  represents the received composite signal.  $F_N$  and  $F_M^{-1}$  are the DFT and IDFT matrix.  $D_M$  is the DWT matrix used during regeneration for SIC. The weak user is recovered after SIC using the equalization and the equivalent demodulation transform given by

$$\hat{x}_{i+1}^p(u) = \text{sgn} [F_M^{-1} (Y_{i+1}^p(u) W_{i,MMSE}^p)],\tag{18}$$

where  $F_M^{-1}$  is an IDFT matrix.

#### 4. Proposed JLC RZF- SIC JDPD SC-FDMA NOMA system

The equalization schemes have a major requirement to guarantee improved multipath channel performance and diminish ISI. The equalization techniques such as ZF and MMSE have an important role to play in mitigating ISI. The commonly used linear equalization schemes such as ZF and MMSE can offer improved performance. However, they are liable to undergo noise amplification and higher detection complexity due to direct matrix inversion during equalization at the receiver with more subcarriers. The MMSE receiver can offer better performance with increased complexity of Signal to Noise Ratio (SNR) estimation and matrix inversion of interference matrix. Equation (6) indicates the interference matrix, which represent the interference from neighboring subcarriers to the desired one. This interference has minimal significance on adjacent subcarriers when the subcarrier distance  $(v - u)$  increases.

In equation (11) the computation of MMSE equalization requires a complexity of  $O(N^3)$  computations. The joint equalization and CFO compensation in JDPD SC-FDMA NOMA can be implemented with low-complexity using BMA denoted as

$$(\Pi)_{u,v} = \begin{cases} (\Omega)_{u,v} & \text{if } |u - v| \leq \tau \\ 0 & \text{if } |u - v| \geq \tau \end{cases},\tag{19}$$

where  $\Pi, \Omega \in c^{N \times N}$ , represents the BMA and full matrix leading to low-complexity interference cancellation. The banded matrix  $\Pi$  corresponds to the entries of joint channel and CFO matrix of  $k^{\text{th}}$  user belonging to  $p^{\text{th}}$  cluster.  $u, v$  specifies the subcarrier of  $u^{\text{th}}$  row and  $v^{\text{th}}$  column and  $\tau$

denotes subcarrier length of the banded-matrix considered during equalization.

The proposed low-complexity JDPD SC-FDMA NOMA utilizing the BMA detects the  $k^{\text{th}}$  strong user data of  $p^{\text{th}}$  cluster through JLC-RZF equalization denoted as

$$\hat{Y}_{DWT,k}^{(p)} = Y_{DWT,k}^{(p)} \psi_{k,RZF}^p. \quad (20)$$

where  $\psi_k^p$  is the JLC-RZF weights obtained through BMA denoted as

$$\psi_k^p = (\Pi_k^{pH} \Pi_k^p + \sum_{p=(l-1)q+1}^{lq} \Pi_l^{kH} \Pi_l^k + (\beta)I_N)^{-1} \Pi_l^{kH}. \quad (21)$$

where  $\beta$  characterizes the regularization parameter.  $\Pi_l^k$  is the JLC-RZF equalization weights obtained through BMA. The banded bandwidth represents the number of subcarriers involved in equalization rather than using an entire set of subcarriers in systems without BMA. After equalization and CFO compensation the data vector of the strong user is estimated and regenerated using the channel information and precoding matrix. The regenerated strong user data is cancelled from the received composite signal using JLC RZF-SIC to obtain the weak user data as

$$Y_{i+1}^p(u) = Y^{(p)}(u) - \psi_i^p D_M \left\{ F_M^{-1} \left\{ F_N \left( \hat{x}_k^p \right) \right\} \right\}, \quad (22)$$

where  $Y^{(p)}(u)$  is the received composite signal.  $F_N$  and  $F_M^{-1}$  are the matrices corresponding to DFT and IDFT matrix.  $D_M$  is the DWT matrix.  $\psi_i^p$  corresponds to the JLC-RZF equalization weights associated with the banded matrix. It should be noted that during SIC in JDPD SC-FDMA NOMA we use a banded matrix for equalization and interference extraction which further simplifies the complexity of the system. Finally, the recovered data after JLC RZF-SIC and JLC-RZF equalization is denoted as

$$\hat{x}_{i+1}^p(u) = \text{sgn} \left[ F_M^{-1} \left( Y_{i+1}^p(u) \right) \psi_{i,JLC-RZF}^p \right] \quad (23)$$

## 5. Simulation results and discussion

Extensive comparative analysis on the proposed JDPD SC-FDMA NOMA over conventional SC-FDMA system is done in this section. In simulations, we consider a vehicular A outdoor channel model consisting of 6 tap Rayleigh fading channels. The channel gain for each multipath component of weak user is chosen 0.3 times the channel gain of the strong user. The fading coefficients are assumed as quasi static for each transmitted data block. The average BER is calculated based on the transmission of  $10^6$  bits of BPSK modulated data. The JDPD SC-FDMA NOMA is

**Table 1.** Simulation parameters.

Description	Parameter
System bandwidth	5 MHz
Modulation	BPSK
CP	20 samples
Subcarrier mapping	localized
Transmitter IDFT size	$M = 512$ symbols
SC-FDMA input block size	128 symbols
User per cluster	2
CFO range	-0.1 to 0.1
Transform	Discrete wavelet transform
Channel model	vehicular A outdoor channel
Noise environment	AWGN
Equalisation	MMSE, RZF

simulated with 512 subcarriers. The user pairing in the form of clusters is done and each cluster is allotted with two users. Furthermore, the users in each cluster share the same set of allotted 128 subcarriers. The simulation parameters are listed in table 1. In simulations we assume that the power allocated to strong user is 0.8 and weak user is 0.2. The CP length chosen is 20 to overcome the ISI induced by the channel due to delay spread in Vehicular A channel. Rather than the values mentioned during simulations, the CFO value used are random variables distributed uniformly over the interval [-0.1 to 0.1]. These values clearly depict the performance of the system in an outdoor environment with multipath characteristics.

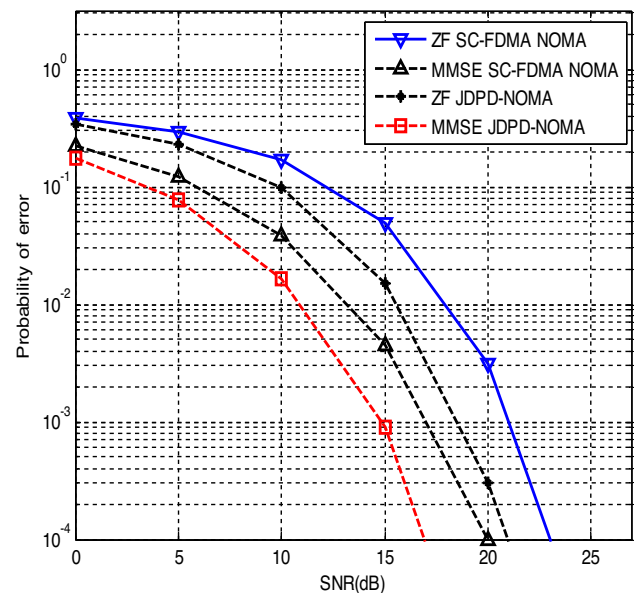


**Figure 3.** A comparative performance analysis of JDPD SC-FDMA NOMA for strong user detection.

### 5.1 BER analysis using different equalization techniques

In this section, the BER performance is studied for conventional and JDPD SC-FDMA NOMA system with normalized CFO. Figure 3 depicts a comparative analysis among JDPD SC-FDMA NOMA with conventional SC-FDMA system. The performance characteristic is plotted for strong user detection. It is observed that MMSE-based detection [28–31] is proficient enough to accomplish superior performance over ZF. It can be noted that the proposed JDPD SC-FDMA NOMA can impact the performance of the equalization technique. This is mainly due to the ability of DWT in exhibiting a sparse representation of the channel under severe multipath channel. The sparsity of the channel characteristics is exploited in the equalization process to improve the system performance over the conventional DFT based system [29]. At BER  $10^{-3}$  JDPD SC-FDMA NOMA accomplishes a 3 dB gain over the SC-FDMA NOMA system. With ZF scheme, a gain of 5 dB is achieved compared to the ZF SC-FDMA NOMA system.

Figure 4 portrays an evaluation between JDPD SC-FDMA NOMA with conventional SC-FDMA system for weak user detection. The weak user is detected through MMSE and SIC of strong user. The plot shows the significance of JDPD SC-FDMA NOMA in accomplishing superior performance over DFT SC-FDMA systems with MMSE detection [28–31]. The proposed system with MMSE achieves 3 dB gain over SC-FDMA NOMA system at BER  $10^{-3}$  in the detection of weak user. This is mainly due to the better localization characteristics of DWT which localizes the signal energy in specific time-frequency

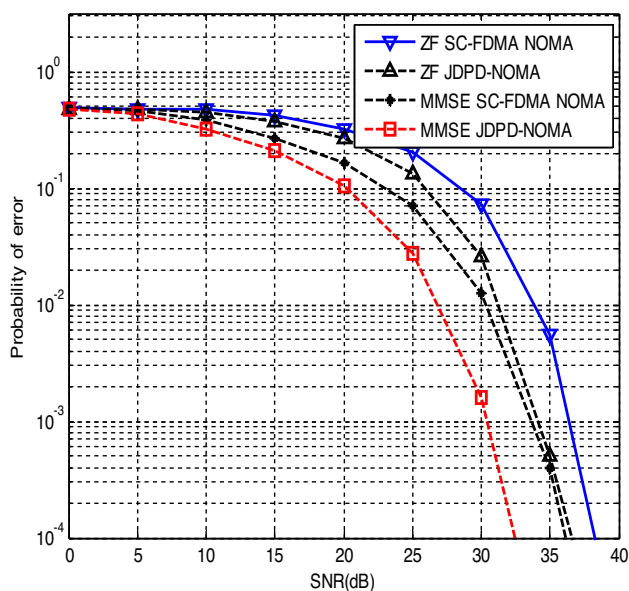


**Figure 4.** A comparative performance analysis of JDPD SC-FDMA NOMA for detecting weak user.

regions. This minimizes ISI and hence improves the system performance.

It is clear from the figure that the performance of ZF SC-FDMA and the ZF JDPD NOMA is same at low SNR regions specifically till 20 dB. At high SNR regions, ZF SC-FDMA NOMA degrades, because the interference power increases at higher values of SNR. Meanwhile, the performance of ZF JDPD NOMA is superior over conventional systems. Moreover, it is clear that for low SNR values, ZF SC-FDMA NOMA acts as a lower bound for JDPD SC-FDMA NOMA. On the other hand, MMSE JDPD NOMA acts as an upper bound in terms of interference handling and performance improvement. The flexibility of DWT to time varying channel conditions rises the performance gain which is a hard task for conventional systems with DFT. This displays the practicality of the proposed system in achieving superior performance than conventional systems.

The influence of CFO on JDPD SC-FDMA NOMA system is portrayed in figure 5 for strong and weak user detection. The CFO value used in the simulation is 0.15. It is observed that conventional system deteriorates at higher SNR values due to ICI induced on the subcarriers with increase in CFO. However, JDPD SC-FDMA NOMA has a SNR gain of 7 dB for both the strong user and weak user detection at BER of  $10^{-3}$ . The extraordinary interference resistant capability of DWT filter structures is capable of providing these performance gain in the proposed JDPD SC-FDMA compared to the conventional systems. At higher SNR values, the performance of the conventional system shows an irreducible error floor leading to poor performance. Whereas, JDPD SC-FDMA system shows a

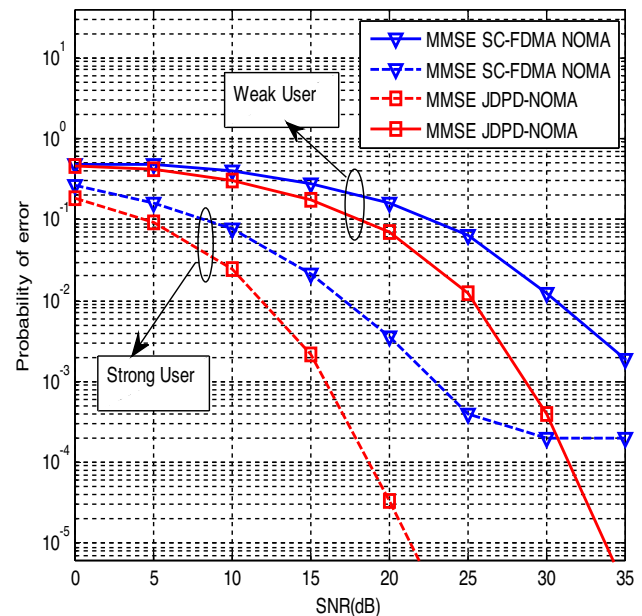


**Figure 5.** BER vs SNR comparison for strong user and weak user detection.



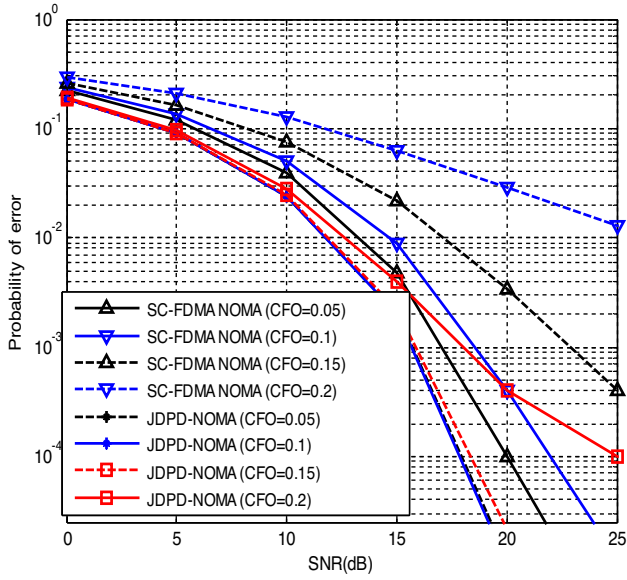


**Figure 6.** A comparative performance analyses of JDPD SC-FDMA NOMA and conventional systems for strong user detection with CFO variation.

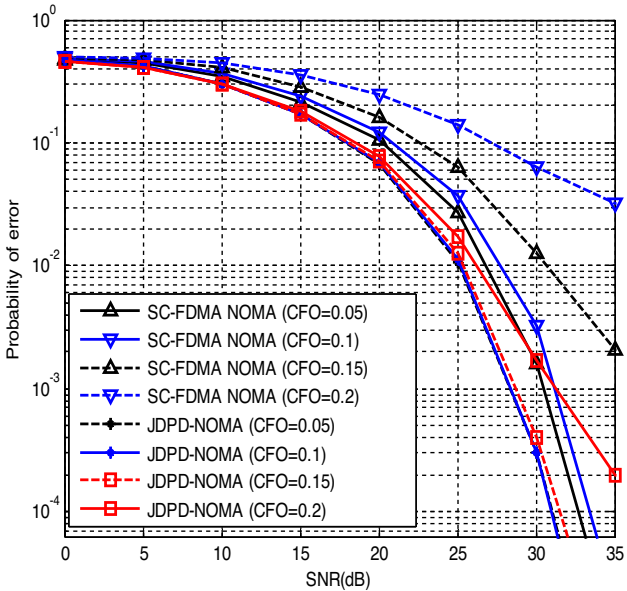


**Figure 7.** A comparative performance analyses of JDPD SC-FDMA NOMA and conventional systems for weak user detection with CFO variation.

two-fold increase in performance gain at higher SNR values validating its improved BER performance.

Figures 6 and 7 compare the proposed system and conventional system with variations in CFO for a strong user and weak user detections, respectively. Owing to CFO variations [28, 29, 32], it is noticed that BER degrades for both the proposed and conventional systems. Nevertheless,

the degradation for JDPD SC-FDMA NOMA is still lower than conventional DFT precoded system. Furthermore, it can be visualized from figures 6 and 7 that the proposed JDPD SC-FDMA NOMA performance is unchanged for CFO variations from 0.05 to 0.15, with 8 dB SNR gain at BER of  $10^{-3}$  for both the strong user and weak user detections. A considerable performance gap occurs for CFO values of 0.2, displaying the dominant interference resistance nature of the JDPD SC-FDMA NOMA system over conventional system.

### 5.2 BER analysis of JDPD SC-FDMA NOMA using proposed JLC-RZF equalization

In this section we analyze the BER performance for conventional and JDPD SC-FDMA NOMA system using JLC RZF equalization. Figures 8 and 9 display the comparison between the proposed JDPD SC-FDMA NOMA with RZF equalization for full compensation. Figure 8 is plotted to identify the optimum value of regularization parameter  $\beta$  [28, 29, 32]. The proper choice of regularization parameter plays a vital role in enhancing the system performance. RZF is a variation of ZF which includes a regularization term to the channel inversion. The regularization parameter reduces the performance degradation owing to noise and achieves improved performance in the presence of channel estimation errors. Hence, proper tuning of the regularization parameter is essential to obtain the required response. From figure 8, it is apparent that the optimum choice is  $\beta = 0.1$ . Hence, for the remaining part of the analysis we consider the value of  $\beta$  as 0.1.

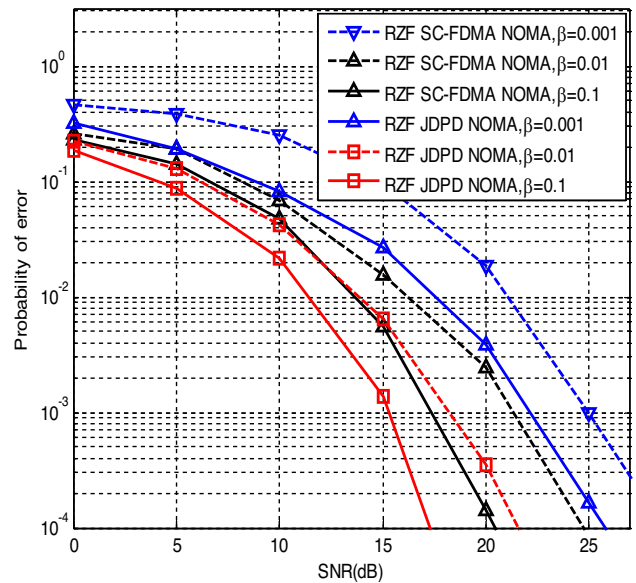


**Figure 8.** A comparative performance analysis of JDPD SC-FDMA NOMA with variations in regularization parameter for strong user detection with full compensation.

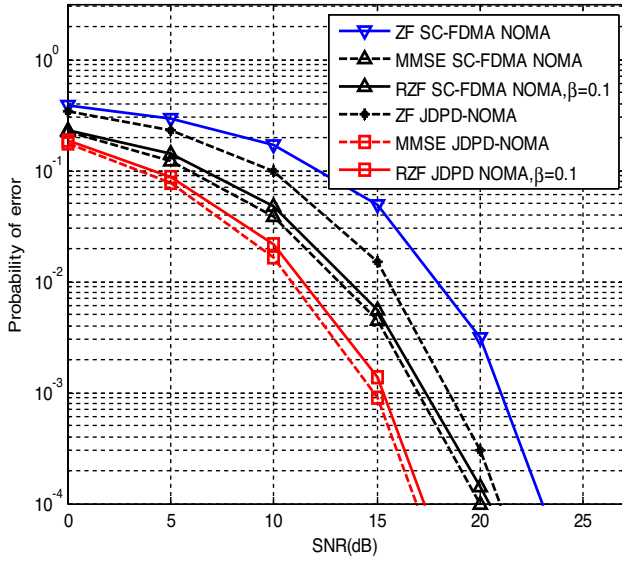


**Figure 9.** A comparative performance analysis of JDPD SC-FDMA NOMA with RZF for strong user detection with full compensation.

The performance of RZF is normally assessed through comparisons with other equalization techniques considering the assumed channel conditions and the level of regularization. In figure 9, RZF is compared with ZF and MMSE to show the significance of RZF in achieving comparatively identical performance similar to MMSE with lower complexity. The performance assessment is accomplished using the value of  $\beta = 0.1$  for both the proposed system and conventional system. The regularization parameter acts as a

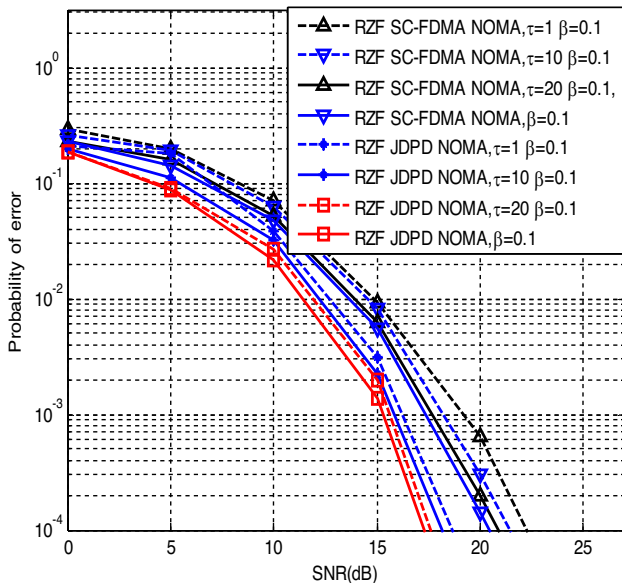
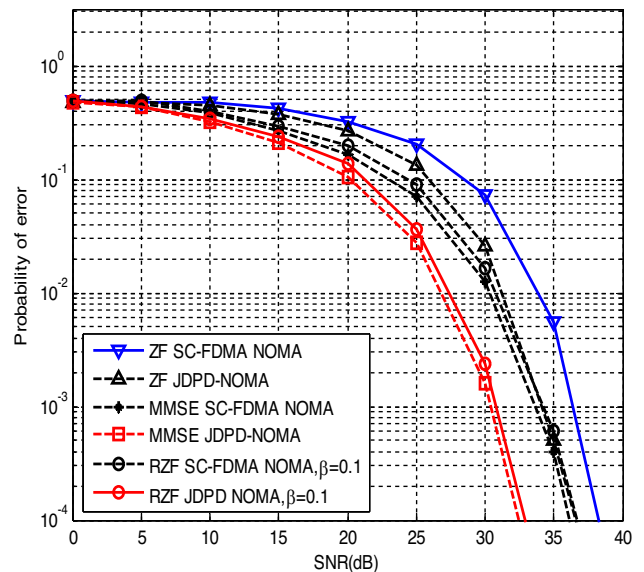


**Figure 10.** A comparative performance analysis of JDPD SC-FDMA NOMA with RZF for strong user detection with variations in banded bandwidth.

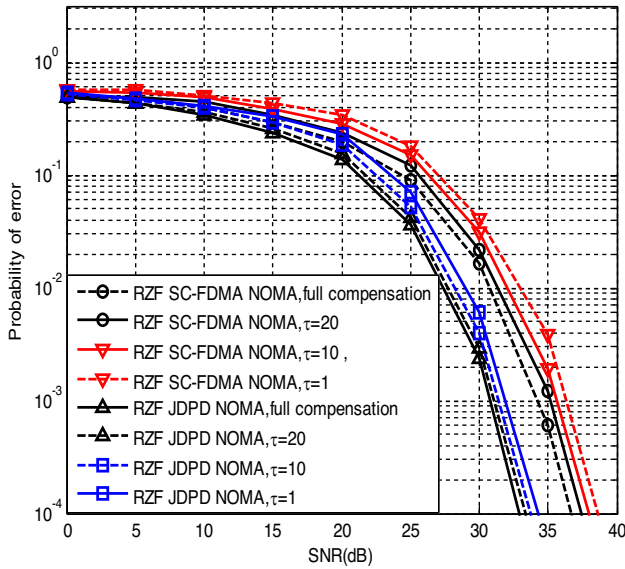
central parameter in regulating the trade-off between interference reduction and noise enhancement. It is evident from the plot, at BER of  $10^{-3}$  RZF JDPD SC-FDMA NOMA achieves an equivalent SNR gain of MMSE based system without the need for SNR estimation and noise power.

Figure 10 illustrates the performance analysis of conventional SC-FDMA NOMA and JDPD SC-FDMA NOMA with proposed JLC RZF for different banded bandwidth. The banded band width  $\tau$  plays a significant role in describing the number of subcarriers involved in achieving improved performance with lower complexity [29, 32]. Figure 10 visualizes that SNR loss of RZF JDPD SC-FDMA NOMA is very minimum at BER of  $10^{-3}$  with banded bandwidth of  $\tau = 20$ . It can be noticed that JLC RZF is capable to achieve superior performance close to full compensation with low complexity.

Figures 11 and 12 illustrate the BER performance of the JDPD SC-FDMA NOMA for detection of weak user. In figure 11, it can be noticed that RZF is capable of attaining equal performance close to MMSE based detection for full compensation [29, 32]. In figure 12, it is noticed that JLC RZF-SIC JDPD SC-FDMA NOMA is capable of detecting the weak user with lower complexity with minimum loss in SNR [32]. It is noted that JLC RZF-SIC JDPD SC-FDMA NOMA with banded bandwidth  $\tau = 20$  is capable of achieving SNR gain of 4 dB compared over conventional system. Henceforth, it is clear that banded bandwidth  $\tau = 20$  is the correct choice for the proposed system for attaining comparatively better performance over full compensation during weak user detection.



**Figure 11.** A comparative performance analysis of JDPD SC-FDMA NOMA with RZF for weak user detection with full compensation.



**Figure 12.** A comparative performance analysis of JDPD SC-FDMA NOMA with RZF for weak user detection with BMA.

### 5.3 BER analysis of JDPD SC-FDMA NOMA under different power allocation strategies

The SC-FDMA NOMA system can achieve uplink performance gains based on the channel gain difference between strong and weak users in each cluster. The channel gain in each cluster plays a vital role in varying the performance of the JDPD SC-FDMA NOMA system. The users are paired with two users in a cluster, where the strong user is considered near the BS and the weak user at a distant point

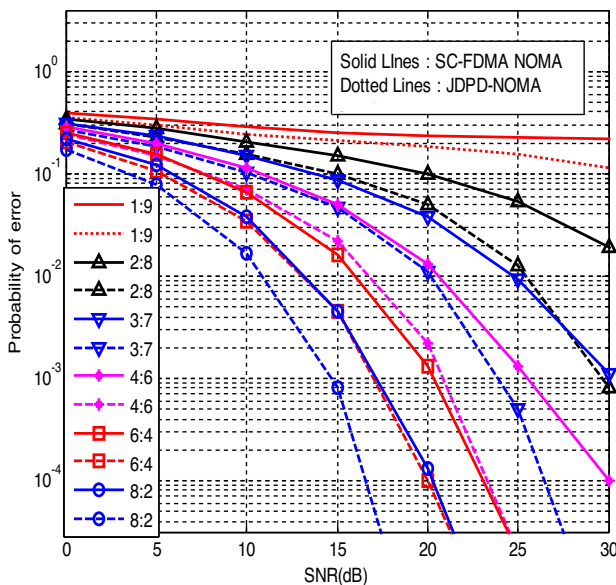


**Figure 13.** A comparative performance analyses of JDPD SC-FDMA NOMA and conventional systems for strong user detection with variation in power ratio.

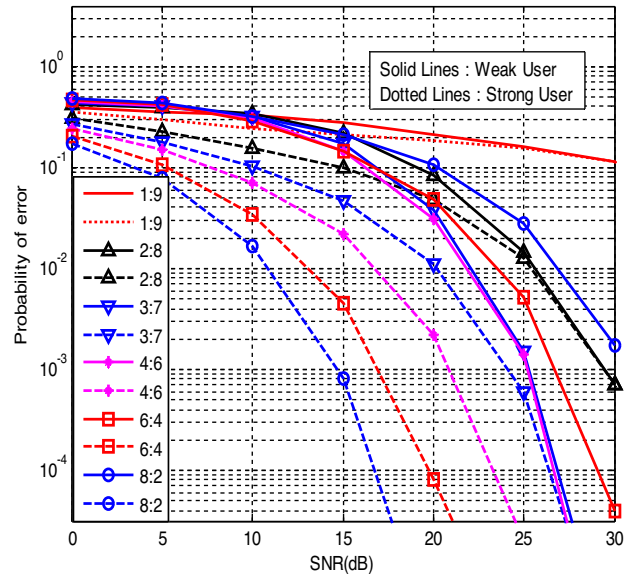


**Figure 14.** Performance comparison of JDPD SC-FDMA NOMA under diverse power allocation schemes for strong and weak users.

from the BS. Based on the user pairing, the strong user exhibits a strong line of sight (LOS) to the BS, and the weak user at a faraway distance exhibits a lower channel gain to the BS. In addition, the power allocation strategies used in the NOMA system also play an essential role in increasing the system performance. Figures 13 and 14 describe the comparison between the proposed and conventional system with dissimilar power allocation strategies with MMSE detection. The user power ratios considered in the plot are 1:9, 2:8, 3:7, 4:6, 6:4, and 8:2.

Figure 13 displays the BER performance for strong user detection at different power allocation ratios [33]. The proposed JDPD SC-FDMA NOMA system achieves diversity gains compared to conventional systems for the power ratio of 1:9, 2:8, and 3:7. For BER of  $10^{-3}$ , the proposed system establishes an SNR gain of 7 dB over conventional system for the power ratio of 3:7. For the proposed system, however, it is witnessed that the performance deteriorates for the strong user with a power ratio of 1:9, leading to a constant error floor. There is performance degradation owing to lower channel gain difference among strong and weak users. Nevertheless, by careful user pairing and by appropriately selecting the near user and far user pair the performance improvement can be obtained.

A comparative BER performance is shown in figure 14 with different fractions of power allocation [33, 34]. Even though high power is allocated to weak user, the proposed system exhibits poor performance in decoding strong and weak users for a power ratio of 1:9. This occurs owing to the small channel gain difference between the weak user and the strong user causing substantial interference to the LOS component leading to poor performance. This

decrease in the channel gain difference diminishes the performance gap among weak and strong users leading to poor BER performance at a power ratio of 1:9.

It is apparent from the figure 14, that the BER performance increases with an increase in power levels allocated to the strong user. At the power ratio of 2:8 and 3:7, the performance gap is large at a low SNR ratio, and the gap is minimal at the high SNR region. A slight increase in the strong user power is required to get this relative performance that strengthens the LOS component with low channel gain differences. At power ratios 4:6, 6:4, and 8:2, the strong users signal strength increases at the BS due to increased strong user power leading to extraordinary performance. The high power allocated to strong users compensates for the adverse effects due to low channel gain difference.

In the case of weak user detection, the power ratios 2:8 and 3:7 offer considerable improvements in the performance compared to the power ratio of 1:9. This performance improvement is due to the improvement in channel gain difference with the increase in weak user power reducing the interference caused by the scattered components on the LOS. However, at the power ratio of 4:6, optimal performance is achieved for both strong and weak user detection. Therefore, the power ratio of 4:6 remains favorable in offering superior performance for both strong and weak users. On the other hand, at power ratios of 6:4 and 8:2, the performance gap increases. The reduction in power allocated to weak users causes reduced performance and fails to compensate the adverse effects due to low channel gain difference.

Figures 13 and 14 illustrate that proper attention is required to select the proposed system's power ratios to achieve significant BER performance. In the performance analysis it is found that the power ratios 4:6 and 6:4 accomplish enhanced BER performance for both strong user and weak user detection over other power ratios. Unfortunately, the power ratios 1:9, 2:8, and 3:7 cannot offer promising BER performance due to the prevailing low channel gain difference. On the other side, power ratio 8:2 offers superior BER performance for strong user detection and poor performance for weak user detection. It is evident that the proposed JDPD SC-FDMA NOMA system arises as a dominant receiver with the power ratios of 4:6 and 6:4 for detecting both strong and weak users while providing superior BER performance.

## 6. Conclusion

NOMA plays a central part in 5G and B5G wireless communication due to its capability in offering increased user capacity and massive machine type communication. In uplink communication user clusters with distinct channel gains are capable of offering higher throughput and BER

performance with optimal power allocation. We have investigated an efficient receiver technique referred as JDPD SC-FDMA NOMA which is robust in achieving superior performance.

Furthermore, the proposed JLC-RZF JDPD SC-FDMA NOMA performs equalization and interference cancellation using low-complexity BMA. The low-complexity JLC-RZF JDPD SC-FDMA NOMA system is compared with traditional SC-FDMA NOMA system to show its significance in achieving significant BER performance under severe CFO variations and multipath channel conditions.

The power allocation policies studied in this paper have resulted in designing best power pattern to achieve improved performance over conventional systems. Regardless of the abundant benefits achieved by incorporating NOMA, the problem associated with SIC error propagation and inter-cell interference is yet to be explored. Hence, the future scope of this paper is to explore better power allocation pattern for dense cellular networks where inter-cell interference is a major problem.

## References

- [1] Rappaport T S, Xing Y, Kanhere O, Ju S, Madanayake A, Mandal S, Alkhateeb A and Trichopoulos G C 2019 Wireless communications and applications above 100 GHz: Opportunities and challenges for 6G and beyond. *IEEE Access*. 7: 78729–78757
- [2] Vaezi M, Schober R, Ding Z and Poor H V 2019 Non-orthogonal multiple access: Common myths and critical questions. *IEEE Wirel. Commun.* 26(5): 174–180
- [3] Wang B, Yuan Y, Han S, Chih-Lin I and Wang Z 2015 Non-orthogonal multiple access for 5G: solutions, challenges, opportunities, and future research trends. *IEEE Commun. Mag.* 53(9): 74–81
- [4] Merin Joshiba J, Judson D and Bhaskar V 2023A Comprehensive Review on NOMA Assisted Emerging Techniques in 5G and Beyond 5G Wireless Systems. *Wirel. Pers. Commun.* 130(1): 2385–2405
- [5] Umehara J, Kishiyama Y and Higuchi K 2012 Enhancing user fairness in non-orthogonal access with successive interference cancellation for cellular downlink 2012 *IEEE International Conference on Communication Systems (ICCS)*, IEEE, 324–328
- [6] Benjebbour A, Saito K, Li A, Kishiyama Y and Nakamura T 2015 Non-orthogonal multiple access (NOMA): Concept, performance evaluation and experimental trials. In: *2015 International conference on wireless networks and mobile communications (WINCOM)*, IEEE, 1–6
- [7] Shalini R B and Stewart S L 2019 Power domain cyclic spread multiple access: An interferenceresistant mixed NOMA strategy. *Int. J. Commun. Syst.* 32(13): e4025
- [8] Judson D and Bhaskar V 2018 Error rate analysis of SIMO-CDMA with complementary codes under multipath fading channels *Wirel. Pers. Commun.* 98: 1663–1677



- [9] Selvaraj K, Anandaraj M, Judson D, Ganeshkumar P and Rajkumar K 2022 A low complexity near optimal signal detection for large scale MIMO SC-FDMA uplink system. *Wirel. Pers. Commun.* 126(1): 231–250
- [10] Al-Imari M, Xiao P, Imran MA and Tafazolli R 2014 Uplink non-orthogonal multiple access for 5G wireless networks. In: *2014 11th international symposium on wireless communications systems (ISWCS)*, IEEE, 781–785
- [11] Selvaraj K, Judson D, Ganeshkumar P and Anandaraj M 2020 Low complexity linear detection for uplink multiuser MIMO SC-FDMA systems. *Wirel. Pers. Commun.* 112: 631–649
- [12] Bachl R, Gunreben P, Das S and Tatesh S 2007 The long term evolution towards a new 3GPP\* air interface standard. *Bell Labs Tech. J.* 11(4): 25–51
- [13] Hsu C Y and Liao H C 2018 Generalised precoding method for PAPR reduction with low complexity in OFDM systems. *IET Commun.* 12(7): 796–808
- [14] Cho L, Liao H C and Hsu C Y 2018 Adjustable PAPR reduction for DFTsOFDM via improved general precoding scheme. *Electron. Lett.* 54(14): 903–905
- [15] Sattar I, Shahid M and Khan M 2015 A review of pre-coding based system to reduce PAPR in OFDMA. *Int J Multidiscip Sci Eng.* 6(2): 34–37
- [16] Baig I 2017 A precoding-based multicarrier non-orthogonal multiple access scheme for 5G cellular networks. *IEEE Access* 5: 19233–19238
- [17] Baig I, ul Hasan N, Zghaibeh M, Khan I U and Saand A S 2017 A DST precoding based uplink NOMA scheme for PAPR reduction in 5G wireless network. In: *2017 7th international conference on modeling, simulation, and applied optimization (icmsao)*. IEEE: 1–4
- [18] Mounir M, Tarrad I F and Youssef M I 2018 Performance evaluation of different precoding matrices for PAPR reduction in OFDM systems. *Internet Technol. Lett* 1(6): e70
- [19] Yang F and Wang X 2017 A novel waveform for massive machine-type communications in 5G in *2017 IEEE wireless communications and networking conference (WCNC)*, IEEE, 1–5
- [20] Li A, Benjebbour A, Chen X, Jiang H and Kayama H 2015 Uplink non-orthogonal multiple access (NOMA) with single-carrier frequency division multiple access (SC-FDMA) for 5G sstems. *IEICE Trans. Commun.* 98(8): 1426–1435
- [21] Judson D, Annie Portia A and Agnel Livingston L G X 2023 Low-complexity Joint Equalization and CFO Compensation in Uplink SC-FDMA NOMA System under Different Power Allocation Strategies. *Emerging Transactions on Telecommunications.* 34(10): 1–18
- [22] Haci H, Zhu H and Wang J, 2015 A novel interference cancellation technique for non-orthogonal multiple access (NOMA) in *2015 IEEE global communications conference (GLOBECOM)*, IEEE 1–6
- [23] Wang X, Labeau F and Mei L 2017 Closed-form BER expressions of QPSK constellation for uplink non-orthogonal multiple access. *IEEE Commun. Lett.* 21(10): 2242–2245
- [24] Al-kamali F S, Dessouky M I, Sallam B M, Shawki F and Abd El-Samie F E 2010 Transceiver scheme for single-carrier frequency division multiple access implementing the wavelet transform and peak-to-average-power ratio reduction methods. *IET Commun.* 4(1): 69–79
- [25] Khan A, Khan S, Baig S, Asif H M and Shin S Y 2019 Wavelet OFDM with Overlap FDE for non-Gaussian channels in precoded NOMA based systems. *Futur Gener. Comput. Syst.* 97: 165–179
- [26] Khan A and Shin S Y 2017 Linear precoding techniques for OFDM-based NOMA over frequency-selective fading channels. *IETE J. Res.* 63(4): 536–551
- [27] Trivedi V K, Ramadan K, Kumar P, Dessouky M I and Abd El-Samie F E 2019 Enhanced OFDM-NOMA for next generation wireless communication: a study of PAPR reduction and sensitivity to CFO and estimation errors. *AEU-International J. Electron. Commun.* 102: 9–24
- [28] Trivedi V K, Ramadan K, Kumar P, Dessouky M I and Abd El-Samie F E 2019 Trigonometric transforms and precoding strategies for OFDMbased uplink hybrid multi-carrier nonorthogonal multiple access. *Trans. Emerg. Telecommun. Technol.* 30(12): e3694
- [29] Al-Kamal F S, Hassan E S, El-Naby M A, Shawki F, El-Khamy S E, Dessouky M I, Sallam B M, Alshebeili S A and Abd El-samie F E 2015 An efficient transceiver scheme for SC-FDMA systems based on discrete wavelet transform and discrete cosine transform. *Wirel. Pers. Commun.* 83: 3133–3155
- [30] Arun Prem Santh J, Judson D, Selvaraj K and Bhaskar V 2022 Improved PAPR reduction using gamma correction in SC-FDMA systems under multipath fading channels. *Wirel. Pers. Commun.* 125(3): 2889–2905
- [31] Judson D, Santh J A P, Kar R and Bhaskar V 2023 Joint PAPR reduction and carrier frequency offset compensation in SC-FDMA systems using modified gamma correction companding. *Sādhanā* 48(3): 123
- [32] Ramadan K, Dessouky M I, Abd El-Samie F E and Fiky A S 2020 Equalization and blind CFO estimation for performance enhancement of OFDM communication systems using discrete cosine transform. *Int. J. Commun. Syst.* 33(3): e3984
- [33] Hassan E S, El-Khamy S E, Dessouky M I, El-Dolil S A and Abd El-Samie F E 2012 PAPR reduction for OFDM signals with unequal power distribution strategy and a reduced-complexity SLM scheme. *J. Cent. South Univ. Technol.* 19(7): 1902–1908
- [34] Ramadan K, Dessouky M I and Abd El-Samie F E 2020 Joint equalization and CFO compensation for performance enhancement of MIMO-OFDM communication systems using different transforms with banded-matrix approximation. *AEU-International J. Electron. Commun.* 119: 153157

Springer Nature or its licensor (e.g. a society or other partner) holds exclusive rights to this article under a publishing agreement with the author(s) or other rightsholder(s); author self-archiving of the accepted manuscript version of this article is solely governed by the terms of such publishing agreement and applicable law.